Behavior of geodesic acoustic mode and limit-cycle oscillation approaching L-H transition in JFT-2M tokamak

T. Kobayashi[1,2], M. Sasaki[3], T. Ido[4], K. Kamiya[5], Y. Miura[5], K. Ida[1], and K. Itoh[6,1]

[1] National Institute for Fusion Science, National Institutes of Natural Sciences, Toki 509-5292, Japan

[2] The Graduate University for Advanced Studies, SOKENDAI, Toki 509-5292, Japan

[3] College of Industrial Technology, Nihon University, Narashino 275-8575, Japan

[4] Research Institute for Applied Mechanics, Kyushu University, Kasuga 816-8580, Japan

[5] National Institutes for Quantum and Radiological Science and Technology, Naka 311-0193, Japan

[6] Institute of Science and Technology Research, Chubu University, Kasugai 487-8501, Japan

E-mail: kobayashi.tatsuya@nifs.ac.jp

Abstract. In this paper, a phenomenology of competing behavior between the geodesic acoustic mode (GAM) and the limit-cycle oscillation (LCO) is presented. Before the LCO occurs, the GAM can grow to the observable amplitude via the turbulent Reynolds stress force. Approaching the L-H transition, the LCO is excited and the GAM decays. In the LCO phase, the GAM driving force is possibly suppressed by the nonlocal turbulence amplitude modulation by the LCO.

1. Introduction

Towards achieving burning plasma in a magnetic confinement device, reinforcing the core plasma performance is mandatory. It is widely acknowledged that a high level of cross-field transport of plasma is driven by plasma turbulence, which hampers access to the burning plasma condition. Of the important physical phenomena expected to be a key for reducing the undesirably large amount of turbulent transport are plasma confinement improvement events. In particular, the L-H transition, at which edge particle and thermal confinements are significantly enhanced, will be useful in next generation devices, including ITER and DEMO.

After the first discovery of the L-H transition in ASDEX [1], the essential roles of non-uniformity of the radial electric field E_r in forming the transport barrier were pointed out both theoretically [2, 3] and experimentally [4, 5]. In addition to the stationary E_r structure at the H-mode plasma edge, the so-called E_r-well, there are multiple oscillating structures that likely contribute to the transport reduction. A representative oscillating E_r structure consists of the zonal flows (ZFs), including their high frequency eigenmode branch, the geodesic acoustic modes (GAMs). Since GAMs are widely reproduced in different experimental devices (see Ref. [6] and references therein), whether GAMs play a role in triggering or at least assisting the L-H transition is intensively debated. It is theoretically predicted that oscillating E_r becomes less effective for turbulence transport suppression as the oscillating frequency increases [7].

In experiment, the impact of GAMs for the L-H transition is discussed. By the

combination effect of instant turbulence suppression by the local shear of E_r, induced by the GAM and global flow drive by the reinforced pressure gradient, the L-H transition is initiated [8]. The limit-cycle oscillation (LCO), which refers to the sequential repetition of the L-H transition and the H-L back transition, is found occasionally to involve the GAM activity [9, 10]. On the other hand, cases showing that the GAM cannot solely trigger the L-H transition are also reported [11]. According to an empirical model [8], the discussion whether the GAM can trigger the L-H transition depends on characteristics, such as the GAM frequency, structure and duration, as well as plasma parameters. For more quantitative and comprehensive understanding, further experimental case studies are necessary.

In this contribution, the GAM behavior approaching the L-H transition led by the LCO is experimentally studied, using a dataset obtained by the heavy ion beam probe (HIBP) [12] in the JFT-2M tokamak. Thanks to the excellent capability of direct detection of the electrostatic plasma potential by the HIBP with high spatiotemporal resolutions, a wide variety of turbulence and radial electric field physics, including the GAM activity [13, 14], the LCO dynamics [15, 16], and the L-H transition mechanism [17, 18, 19], has so far been studied in JFT-2M. However, the interrelation among the GAM, the LCO, and the L-H transition has not been explicitly discussed. In particular, a phenomenology of competing relation between the GAM and the LCO is introduced here. The GAM driving force induced by the turbulence Reynolds stress is significantly weakened once the LCO appears before the L-H transition. Since the excited locations

of the GAM and the LCO are different, the interaction between them is considered to be nonlocal. A possible role of the inward turbulence spreading is shown.

2. Results

Experiments were performed on the JFT-2M tokamak (the major radius of $R = 1.3$ m and the averaged minor radius of $a = 0.3$ m). The target plasma conditions are as follows: a toroidal magnetic field of $B_{\rm t} = 1.17$ T, a plasma current of $I_{\rm p} = 190$ kA, a neutral beam (NB) heating power of $P_{\rm NB} = 750$ kW, a line averaged electron density of $\langle n_{\rm e} \rangle = 1.1 \times 10^{19}$ m^{-3}, and a safety factor at the flux surface enclosing 95% of the total poloidal flux of q_{95} =2.9. This NB heating power corresponds to the marginal L-H transition power threshold condition for this density range. The divertor is operated with an upper single-null configuration with the ion ∇B drift direction towards the X-point.

Fluctuations on the electrostatic potential and the plasma density are diagnosed by the heavy ion beam probe (HIBP) [12]. The temporal resolution of HIBP is $\Delta t = 1$ μs. Four spatial positions are simultaneously measured with a channel separation projected on the outer mid-plane of ~ 2.5 mm. This distance is smaller than the characteristic length of E_r variation ($O(1$ cm) as shown in Fig. 3 (b)). Radial extent of the sampling volume is ~ 6 mm so that the adjacent sampling volumes partially overlap. In gradient calculation for E_r and the density gradient, channels at both ends of the array are used. The radial positions of the measurement are scanned by adjusting the HIBP operational

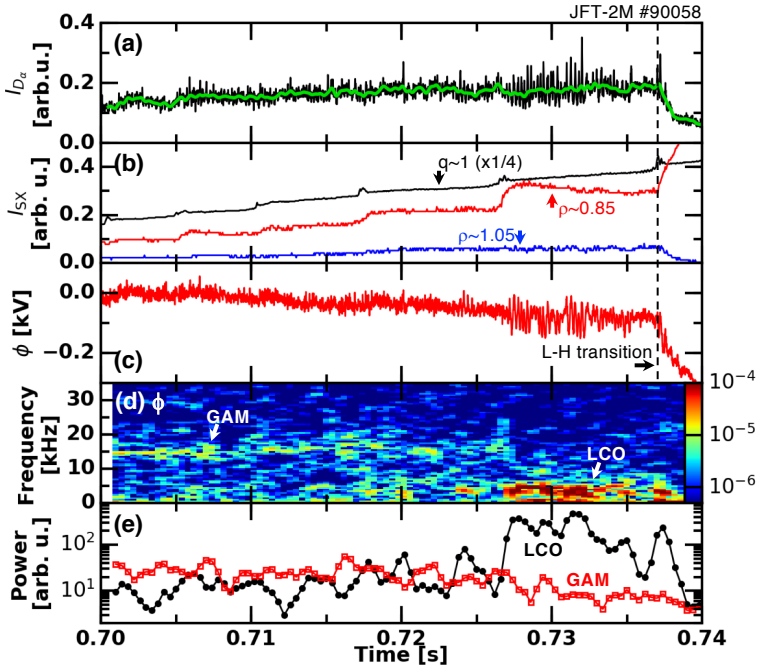

Figure 1. Time evolutions of (a) D_α emission intensity, (b) soft X-ray emission intensity, (c) electrostatic potential, (d) spectrogram of electrostatic potential, and (e) fluctuation powers of LCO and GAM. Radial position of the HIBP is $r - a \sim -4.5$ cm. L-H transition occurs at $t \equiv t_{\rm LH} \sim 0.737$ s in this discharge, as shown by vertical dashed line.

parameters. By a shot-by-shot position scan, the edge region of $-5 < r - a < 0$ cm, where r is the radial coordinate, is measured.

Figure 1 shows the time evolution of the D_α emission intensity, the soft X-ray emission intensity, the electrostatic potential, the spectrogram of electrostatic potential, and the fluctuation powers of the GAM and the LCO. The time window used for the Fourier transform is 2 ms, which is shifted every 0.4 ms. The time label of the spectrogram is given for the center of the time window. The radial position of the HIBP is $r - a \sim -4.5$ cm. Note that this position labeling is according to the equilibrium calculation at $t = 0.72$ s. The last closed flux surface moves inward slightly in time,

which causes an outward HIBP position shift approximately at the rate of 1 mm/10 ms. The NB heating begins at $t = 0.7$ s, after which the GAM is excited at $f \sim 15$ kHz. The typical thermalization time for the NBI fast ions is ~ 50 ms. As time passes, the soft X-ray emission intensities at different codes gradually increase, which reflect the plasma temperature increment. This accretion is also confirmed by the charge exchange recombination spectroscopy for the ion temperature measurement [20] (not shown here). In the edge region, the ion temperature and the electron temperature are found to be in the same order of magnitude of $O(100$ eV). Theoretically predicted GAM frequency is consistent with the observed GAM frequency as shown in [13, 14]. In the later phase, the LCO is excited at $f \sim 4.5$ kHz and the GAM decays. At $t = 0.737$ s, the L-H transition occurs and the LCO disappears. The fluctuation power in Fig. 1 (e) is defined as $\int_{f_1}^{f_2} df S(f)$, where $S(f)$ is the auto power spectrum of the electrostatic potential fluctuation. Here, f_1 and f_2 correspond to the frequency range of the GAM ($f_1 = 10$ kHz and $f_2 = 20$ kHz) and the LCO ($f_1 = 2$ kHz and $f_3 = 7$ kHz). As shown in Fig. 1 (e), particularly in $0.72 < t < 0.73$ s, the GAM power and the LCO power anti-correlate in time. Once the LCO becomes significant at $t \sim 0.727$ s, the GAM is completely suppressed. It should be noted that the LCO seen in this radial location, 4.5 cm inside the separatrix, is induced by a potential oscillation on the plasma surface, which may be caused by the periodic change in the outward flux to the scrape-off layer region. Radial electric field oscillation only exists at the very edge region of $r - a > -2$ cm, where the E_r-well structure appears after the L-H transition. Therefore,

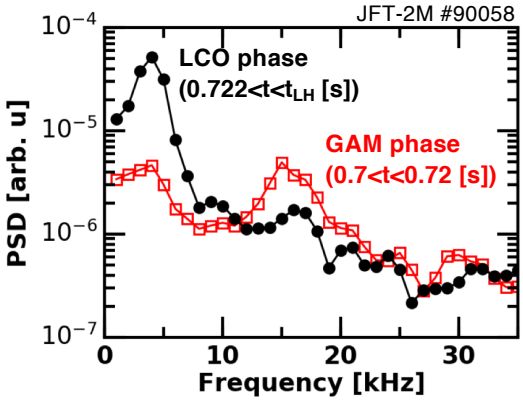

Figure 2. Time averaged power spectral densities of electrostatic potential in GAM phase and LCO phase.

the competition between the GAM and the LCO is not a local phenomenon. A possible mechanism of the nonlocal interaction between the GAM and the LCO is presented in the last part of the paper.

The time averaged power spectrum density of the potential fluctuation is shown in Fig. 2. Here, the time periods of the GAM and the LCO are defined as $0.7 < t < 0.72$ s and $0.722 < t < t_{\rm LH}$ s, respectively, where $t_{\rm LH}$ is the time instance of the L-H transition that is shot dependent. In the LCO phase, the GAM amplitude becomes less pronounced.

The radial profiles of the equilibrium quantities are shown in Figs. 3 (a) and (b). The HIBP signal intensity $I_{\rm HIBP}$, shown in Fig. 3 (a), is proportional to the local electron density if the pass-integral effect is less significant at the edge. This condition is not satisfied in $r - a < -2$ cm, where the HIBP probe beam damping is substantial (shown by dotted curves). Focusing on the edge plasma, the density gradient is gradually steepened as time passes. In the earlier phase of the L-mode, the radial electric field

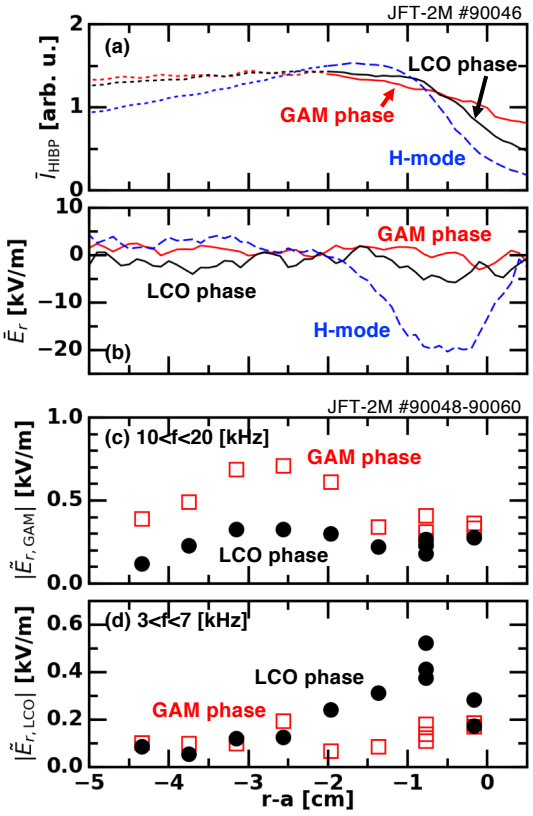

Figure 3. Radial profiles of (a) HIBP signal intensity, (b) radial electric field, (c) GAM amplitude, and (d) LCO amplitude in GAM phase and LCO phase. Radial profiles of HIBP signal intensity and radial electric field in H-mode are also shown in (a) and (b) as references.

profile is nearly flat at $r - a > -2$ cm, where the E_r-well structure forms after the L-H transition (Fig. 3 (b)). In the LCO phase, although not very clearly shown, a small bump forms at this position.

Figures 3 (c) and (d) show the radial profiles of oscillation amplitudes in the radial electric field for the GAM and LCO, respectively. The GAM peaks at $r-a \sim -3$ cm, and the amplitude decays as the position approaches at the edge. Since the GAM emerges away from the E_r-well and the pedestal structures in the H-mode, a direct contribution of the GAM in initiating the L-H transition [8] seems not to be the case. In the LCO phase,

the GAM amplitude nearly halves. Instead, the LCO occurs at the lower frequency of $f \sim 4.5$ kHz at the E_r-well position of $r - a \sim -1$ cm. As discussed in Refs. [15, 16], the LCO was found to be a periodic generation/decay of a moderate transport barrier by this localized E_r oscillating structure. It should be noted that the amplitudes of the GAM and the LCO ($< O(1$ kV/m$)$) are one order of magnitude smaller than the depth of the E_r-well that emerges after the L-H transition. Since the spatial scales of those structures (GAM, LCO, E_r-well) are comparable, impact of the GAM and the LCO on turbulence suppression (shown below) and confinement improvement is less significant compared to the E_r-well structure in the H-mode. Furthermore, oscillating E_r structure was found to be less effective for turbulence suppression as discussed in [7]. Therefore, the GAM and the LCO are considered to play a minor role for triggering the L-H transition. Rather, a possible excitation mechanism for the E_r-well structure was presented as imbalance of the neoclassical force and a turbulent driven wave convection [18, 5].

It is worthwhile to compare the impact of the density profile variation on the dynamics for the GAM and the LCO. The inverse density gradient length estimated from the HIBP intensity profile, $L_{\rm n}^{-1} \equiv -I_{\rm HIBP}^{-1} \nabla I_{\rm HIBP}$, is compared to the normalized radial electric field, eE_r/T, where e is the electron charge and T is the plasma temperature. For the GAM, $|\tilde{L}_{\rm n,GAM}^{-1}|/(e|\tilde{E}_{r,\rm GAM}|/T) \sim 0.4$, while for the LCO, $|\tilde{L}_{\rm n,GAM}^{-1}|/(e|\tilde{E}_{r,\rm GAM}|/T) \sim 2$. Therefore, in the LCO dynamics, the density profile modulation is more important than in the GAM dynamics. Rather, the GAM is driven by the turbulence.

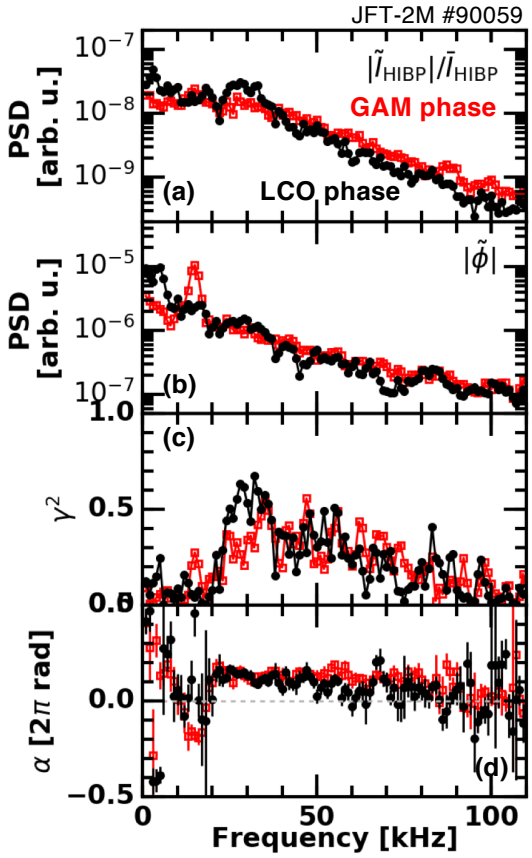

Figure 4. Time averaged spectra of (a) HIBP intensity, (b) electrostatic potential, (c) squared cross coherence and (d) cross phase between HIBP intensity and electrostatic potential at $r - a \sim -2$ cm in GAM phase and LCO phase.

In order to discuss the mechanism of switching between the GAM and the LCO, turbulence properties are analyzed. Figures 4 (a) and (b) show the power spectra of the HIBP intensity (i.e., a proxy of density) and the electrostatic potential in the GAM phase and the LCO phase. Turbulence spectral shapes are nearly unchanged in both phases. Squared cross coherence γ^2 and cross phase between the HIBP intensity and the electrostatic potential α are shown in Figs. 4 (c) and (d), respectively. They also remain qualitatively the same in both phases. A slightly positive phase difference corresponds

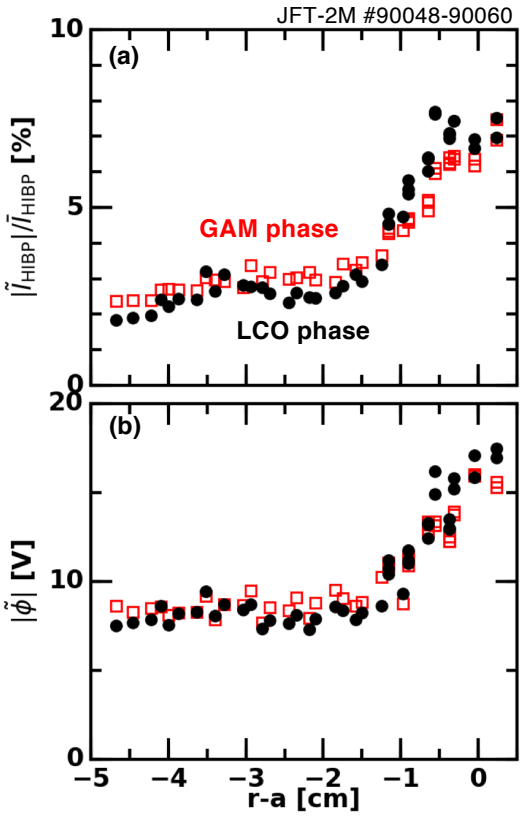

Figure 5. Radial profiles of turbulence amplitude ($40-110$ kHz) in (a) HIBP intensity, (b) electrostatic potential in GAM phase and LCO phase.

to the linearly unstable drift wave-type turbulence.

Radial profiles of the turbulence amplitude are shown in Fig. 5. Both quantities show similar profile shapes, where the turbulence amplitude increases, approaching the edge. The fluctuation amplitude of the electrostatic potential normalized by the plasma temperature, i.e., $e|\tilde{\phi}|/T$, is $5-10$ %, therefore the Boltzmann relation $e|\tilde{\phi}|/T = |\tilde{n}_e|/\bar{n}_e$ is approximately satisfied. According to the turbulence observation, a possibility that the GAM-LCO transition/competition is induced by a drastic change in turbulence property is now excluded.

As described in Ref. [14], the excitation mechanism of the GAM in the JFT-

2M tokamak was identified as the turbulent Reynolds stress modulation. In the nonlinear excitation of the GAM by the turbulent Reynolds stress, a seed perturbation of sheared poloidal flow is amplified by the Reynolds stress modulation of the background turbulence at the GAM frequency. The Reynolds stress modulation is induced through the modulations in the amplitude and wavenumber of turbulence caused by the sheared poloidal flow perturbation itself. This process is called the modulational instability [21]. The Reynolds stress modulation is predominantly caused by the turbulence radial wavenumber. In Ref. [14], the Reynolds stress modulation was directly estimated by using the conditional average. In order to improve the signal-to-noise ratio, the time period in which the GAM amplitude was larger than a threshold value was analyzed. However, in this paper, the conditional average is not applied because the Reynolds stress modulation in the LCO phase, in which the GAM amplitude is mostly low, needs to be obtained. In addition, evaluation of quantities having physical units are abandoned because of lack of signal intensity in the LCO phase. Instead, squared cross coherence γ^2 between the electrostatic potential and the turbulence radial wavenumber is calculated as a proxy of the turbulent Reynolds stress in the GAM phase and the LCO phase, as shown in Fig. 6. Here the turbulence radial wavenumber is estimated from the phase difference between two HIBP intensity signals recorded at two neighboring channels, separated radially and poloidally. Since the poloidal wavenumber modulation is found to be negligibly small, this quantity directly reflects the radial wavenumber modulation. The squared cross coherence peaks at the GAM frequency ($\sim$ 15 kHz) in the GAM

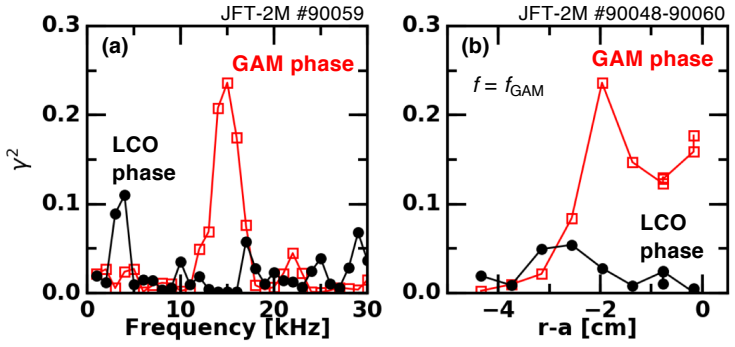

Figure 6. (a) Squared cross coherence between electrostatic potential and turbulence radial wavenumber at $r - a \sim -2$ cm and (b) its radial profiles at GAM frequency in GAM phase and LCO phase.

phase, while the peak disappears in the LCO phase. Spatial distribution of the squared cross coherence at the GAM frequency is shown in Fig. 6 (b). The GAM driving force is the radial gradient of the Reynolds stress, that is the spatial accumulation of the poloidal momentum. The steep gradient in the squared cross coherence at $r - a = -3$ cm is therefore considered to be responsible for driving the GAM, where its amplitude peaks, as shown in Fig. 3 (c). (In Ref. [14], a qualitatively similar discussion was directly had, based on the Reynolds stress modulation amplitude.) On the contrary, the strong drive of the GAM disappears in the LCO phase. In the modulational instability process, the disappearance of GAM drive in the absence of the GAM oscillating component is legitimate. In the LCO phase, γ^2 at the LCO frequency is less prominent. According to the direct estimation of the Reynolds stress force accounting the effective inertia enhancement in the toroidal plasma [5], the Reynolds stress was confirmed to play a minor role in the LCO drive [15, 16]. This means that the LCO is not a low frequency zonal flow.

It is curious that the GAM driving force drastically changes while the turbulence properties do so only slightly. A direct interaction from the LCO to the GAM might exist, which can hamper the latter to grow. The LCO is not driven by turbulence via the Reynolds stress as mentioned above. Therefore, the scenario that the GAM driving energy is fully consumed by the LCO is not the case. Although the LCO is excited at the very edge ($r - a \sim -1$ cm), the impact on the turbulence amplitude propagates towards the core through the turbulence spreading [22, 23]. Figure 7 shows the turbulence amplitude response, reproduced using three different shots. The conditional average [16] is used to extract the reproducible events from a large amplitude of random noise, using the LCO component on the D_α emission signal, which is regarded to be the reference. The LCO in E_r is only prominent at the edge, as shown in Fig. 3 (d). However, turbulence modulation propagates inward with a speed of 900 m/s. This turbulence modulation has an amplitude of up to $10 - 20$ % with respect to the equilibrium turbulence amplitude. The turbulence modulation caused by the LCO propagates to the GAM excitation region ($r - a \sim -3$ cm), and the GAM drive seems to be affected. A possible interpretation of the competition between the LCO and the GAM is given as follows: Because of the low plasma density, the thermalization time for the NBI fast ions is slow as $\sim$ 50 ms. After the NB injection starts, the plasma parameters gradually approach to the L-H transition condition. In the marginal condition before the L-H transition, the LCO is eventually excited. Once the LCO activity emerges, the above-mentioned nonlocal interaction between the LCO and the GAM occurs, and the

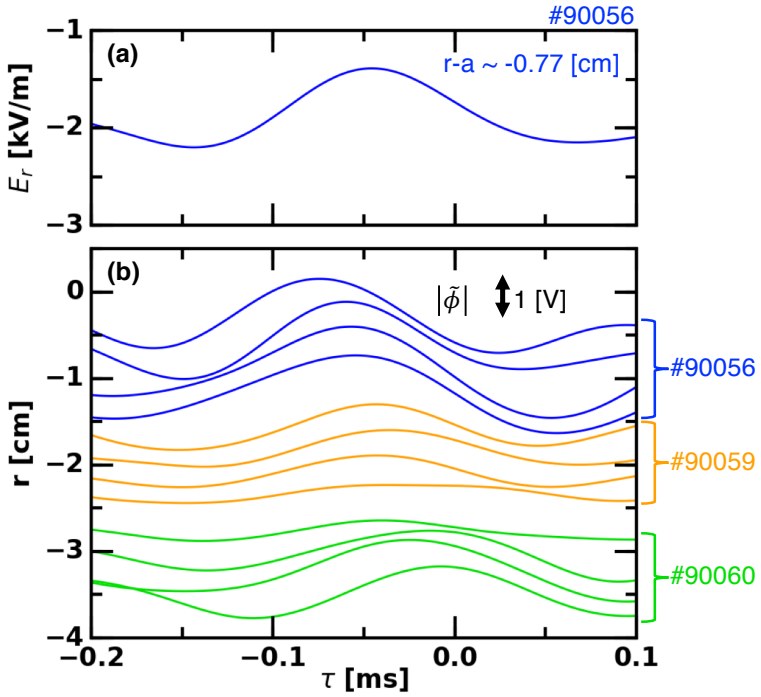

Figure 7. (a) Radial electric field modulation at LCO frequency and (b) spatial propagation of turbulence amplitude ($40 - 110$ kHz) obtained by conditional average.

GAM is suppressed. The particular mechanism of how the GAM is suppressed is not determined in this paper. Further theoretical and numerical approaches are necessary to identify the effect of slow turbulence modulation on the GAM drive.

3. Summary

In this paper, the interrelation among the GAM and the LCO before the L-H transition was, investigated based on the HIBP measurement in JFT-2M. In the case of JFT-2M, the GAM decayed as the LCO was excited, approaching the L-H transition. Although the turbulence properties were maintained in both the GAM and LCO phases, the GAM driving force was significantly suppressed in the latter phase. Turbulence

amplitude modulation, originated by the LCO away from the GAM excitation region, was considered to be a candidate for the disturbance of the GAM excitation. For understanding the physical mechanism of this observation, further theoretical and numerical studies are necessary.

Acknowledgments

Authors acknowledge the late S.-I. Itoh, the late H. Maeda, Y. Hamada, M. Mori, Y. Kamada, and K. Hoshino for strong support. This work is partly supported by the Grant-in-Aid for Scientific Research of JSPS (17K14898, 21K13902).

Data availability

The data that support the findings of this study are available from the corresponding author upon reasonable request.

References

[1] F Wagner, G Becker, K Behringer, D Campbell, A Eberhagen, W Engelhardt, G Fussmann, O Gehre, J Gernhardt, G v Gierke, *et al* 1982 *Phys. Rev. Lett.* **49** 1408

[2] K Itoh and S-I Itoh 1996 *Plasma Phys. Control. Fusion* **38** 1

[3] P W Terry 2000 *Rev. Mod. Phys.* **72** 109

[4] R A Moyer, K H Burrell, T N Carlstrom, S Coda, R W Conn, E J Doyle, P Gohil, R J Groebner, J Kim, R Lehmer, *et al* 1995 *Phys. Plasmas* **2** 2397

[5] T Kobayashi 2020 *Nucl. Fusion* **60** 095001

[6] G D Conway, A I Smolyakov, and T Ido 2022 *Nucl. Fusion* **62** 013001

[7] T S Hahm, M A Beer, Z Lin, G W Hammett, W W Lee, and W M Tang 1999 *Phys. Plasmas* **6** 922–926

[8] L G Askinazi, A A Belokurov, V V Bulanin, A D Gurchenko, E Z Gusakov, T P Kiviniemi, S V Lebedev, V A Kornev, T Korpilo, S V Krikunov, *et al* 2017 *Plasma Phys. Control. Fusion* **59** 014037

[9] G D Conway, C Angioni, F Ryter, P Sauter, J Vicente, and ASDEX Upgrade Team 2011 *Phys. Rev. Lett.* **106** 065001

[10] W Zhong, X Zou, Z Shi, X Duan, M Xu, Z Yang, P Shi, M Ziang, G Xiao, X Song, *et al* 2017 *Plasma Sci. Technol.* **19** 070501

[11] C Silva, J C Hillesheim, L Gil, C Hidalgo, C F Maggi, L Meneses, E R Solano, and JET Contributors 2019 *Plasma Phys. Control. Fusion* **61** 075007

[12] T Ido, Y Hamada, A Nishizawa, Y Kawasumi, Y Miura, and K Kamiya 1999 *Rev. Sci. Instrum.* **70** 955

[13] T Ido, Y Miura, K Kamiya, Y Hamada, K Hoshino, A Fujisawa, K Itoh, S-I Itoh, A Nishizawa, H Ogawa, *et al* 2006 *Plasma Phys. Control. Fusion* **48** S41

[14] T Kobayashi, M Sasaki, T Ido, K Kamiya, Y Miura, Y Nagashima, K Ida, S Inagaki, A Fujisawa,

S-I Itoh, *et al* 2018 *Phys. Rev. Lett.* **120** 045002

[15] T Kobayashi, K Itoh, T Ido, K Kamiya, S-I Itoh, Y Miura, Y Nagashima, A Fujisawa, S Inagaki, K Ida, *et al* 2013 *Phys. Rev. Lett.* **111** 035002

[16] T Kobayashi, K Itoh, T Ido, K Kamiya, S-I Itoh, Y Miura, Y Nagashima, A Fujisawa, S Inagaki, K Ida, *et al* 2014 *Nucl. Fusion* **54** 073017

[17] T Ido, K Kamiya, Y Miura, Y Hamada, A Nishizawa, and Y Kawasumi 2002 *Phys. Rev. Lett.* **88** 055006

[18] T Kobayashi, K Itoh, T Ido, K Kamiya, S-I Itoh, Y Miura, Y Nagashima, A Fujisawa, S Inagaki, K Ida, *et al* 2016 *Sci. Rep.* **6** 30720

[19] T Kobayashi, K Itoh, T Ido, K Kamiya, S-I Itoh, Y Miura, Y Nagashima, A Fujisawa, S Inagaki, and K Ida 2017 *Sci. Rep.* **7** 14971

[20] K Ida, S Hidekuma, Y Miura, T Fujita, M Mori, K Hoshino, N Suzuki, T Yamauchi, and JFT-2M Group 1990 *Phys. Rev. Lett.* **65** 1364

[21] P H Diamond, S-I Itoh, K Itoh, and T S Hahm 2005 *Plasma Phys. Control. Fusion* **47** R35

[22] T S Hahm, P H Diamond, Z Lin, K Itoh, and S-I Itoh 2004 *Plasma Phys. Control. Fusion* **46** A323

[23] X Garbet, Y Sarazin, F Imbeaux, P Ghendrih, C Bourdelle, Ö D Gürcan, and P H Diamond 2007 *Phys. Plasmas* **14** 122305